A Comprehensive Study of Exotic Baryons with CLAS off of a Proton Target

V. Kubarovsky (co-spokesperson), J. Cummings, P. Stoler
Rensselaer Polytechnic Institute

V. Burkert, L. Guo, D. Weygand (co-spokesperson, local contact)
Jefferson Lab

J. Price (co-spokesperson), B. Nefkens
UCLA

M. Anghinolfi, M. Battaglieri, R. De Vita, M. Giannini,
M. Osipenko, G. Ricco, M. Ripani,
E. Santopinto, M. Taiuti
Istituto Nazionale di Fisica Nucleare and Università di Genova

I. Strakovsky
George Washington University

M. Holtrop
University of New Hampshire

M. Khandaker, C. Salgado
Norfolk State University

E. Pasyuk,
Arizona State University

D. Carman, K. Hicks,
Ohio University

P. Eugenio, A. Ostrovidov
FSU

C. Djalali, R. Gothe, D. Tedeschi, M. Wood
Univ. of South Carolina

and the CLAS collaboration

Abstract

We propose to conduct a systematic, high statistics study of the $\Theta^+(1540)$ using the CLAS detector and the energy-tagged photon beam in Hall B. By increasing the sensitivity over previous experiments in CLAS, a more comprehensive understanding of the pentaquark phenomena may be obtained. This proposed experimental run is directed at the exploration of reaction mechanisms for the production of the Θ^+. We also plan to search for the predicted exotic Ξ states, for which evidence has been seen in experiment NA49 at CERN. In addition, the entire Ξ resonance spectroscopy in photoproduction up to a mass of nearly 2 GeV/c^2 can be investigated. This part in particular requires an electron beam with an energy of at least 5.7 GeV, or higher if available. An essential addition to CLAS is a new start counter, a detector to measure the production time of each track individually , thus reducing accidental triggers, and allowing a tagged photon flux of at least 5×10^7 photons/second. In a 40 day running period, a raw sensitivity of nearly 300 events/pb will be obtained.

Contents

Part I
The Study of the Θ^+

1 Introduction

The recent discovery of the Θ^+ baryon [1, 2, 3, 4, 6, 7] with strangeness +1 and doubly–strange quadruplet of baryons Ξ_5 [8] has opened a new era in baryon spectroscopy. Jefferson Lab has been at the forefront of these exciting developments. In addition to our observation of the Θ^+ on the deuteron, we were the first to observe Θ^+ production on proton targets. However, this is only the first step to understanding what we actually have discovered. So far only the Θ^+ and Ξ_5 masses are known, and we have only experimental limits on the widths of these particles. The spins, parities, branching ratios, production cross sections, and anomalous magnetic moments of these particles are practically unknown. The results thus far obtained are quite striking, and already raise interesting issues about the Θ^+ production mechanisms. These issues will be revisited later when the analysis of the previous CLAS data which led to the observation of the Θ^+ on a proton target will be discussed.

This proposal seeks to measure the photo-production of the Θ^+, and other pentaquark states on a proton target with an order of magnitude greater statistical precision than our previous experiments. The determination of the Θ^+ and Ξ_5 quantum numbers and their production mechanisms will be the primary goals. Additionally, this and future experiments will continue the search for the missing members of the baryon antidecuplet suggested in the pioneer papers [9, 10] involving a series of theoretical models of pentaquark families, which attempt to explain the nature of the Θ^+ and to predict new particles [11, 12, 14, 15, 18, 17, 20, 13, 16, 21, 22, 23, 24, 25, 26]. The main conclusion is that the new generation of experiments needs to move from the discovery phase to the determination of the major properties of the pentaquark family.

A proton target has the obvious advantage over nuclear targets in that the proton data can be analyzed theoretically with higher confidence, and will simplify the determination of the quantum numbers from the analysis of the angular distributions and/or differential cross sections. The theoretical estimates of the total production of the Θ^+ baryons suggest that the cross section from the proton target is of the same order as from the neutron ([28, 29] or significantly larger (see for example [31]). As of now only one cross section measurement, by the SAPHIR collaboration, has been reported for Θ^+ production. They estimated the $\gamma p \to \bar{K}^0\Theta^+$ cross section as 200 nb in the photon energy range from 1.7 to 2.6 GeV. This cross section is anomalously large - similar to the cross section for ϕ photo-production. Such a large cross section is difficult to accommodate in any production model, and needs corroboration.

The main physics goals of this and future experiments with the proton target are:

1. Measurement of the differential and total cross section of the reactions $\gamma p \to \bar{K}^0\Theta^+$, $\gamma p \to \pi^+ K^-\Theta^+$, $\Theta^+ \to nK^+, pK^0$.

2. Determination of the Θ^+ mass with high accuracy.

3. Measurement of the Θ^+ width.

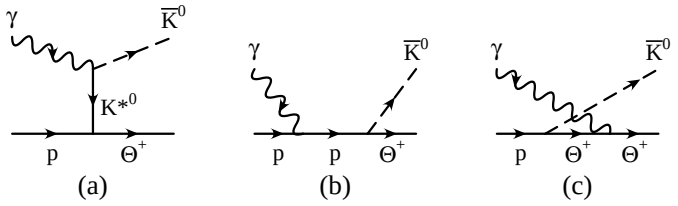

Figure 1: Possible Feynman diagrams for the $\gamma p \to \bar{K}^0 \Theta^+$ reaction.

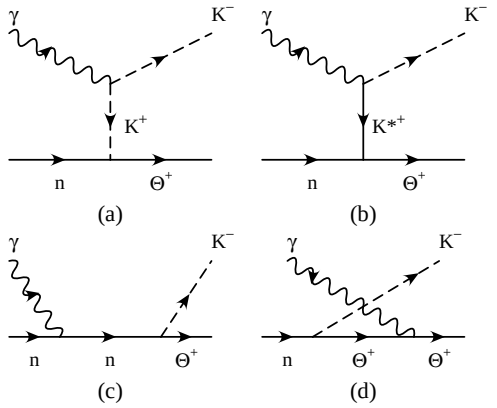

Figure 2: Possible Feynman diagrams for the $\gamma n \to K^- \Theta^+$ reaction.

4. Determination of the Θ^+ parity.
5. Determination of the Θ^+ spin using its decay angular distributions.
6. Search for the Ξ_5 in the photo-production reaction.
7. Search for the missing members of the baryon antidecuplet, as well as their isospin partners, in photo-production reactions.

2 Estimating the Θ^+ production cross sections.

2.1 Hadronic Models with Effective Lagrangians

Estimates of the total and differential cross section for the reactions $\gamma p \to \bar{K}^0 \Theta^+$ and $\gamma n \to K^- \Theta^+$ have been carried out in hadronic models with effective Lagrangians [28, 29, 30, 31, 32]. There are some ambiguities associated with reaction mechanisms, interactions, and the Θ^+ structure in these models. However, within acceptable approximations and ranges of the unknown parameters, it is possible to make conclusions about the behavior of the total and differential cross sections as a function of the kinematics variables, and more importantly as a function of the quantum numbers of the Θ^+ baryon.

Possible Feynman diagrams of Θ^+ production mechanisms from the proton and from the neutron target are shown in Figs. 1 and 2 (see reference [31]). Predictions for the cross sections for the reactions $\gamma p \to \bar{K}^0 \Theta^+$ reaction and $\gamma n \to K^- \Theta^+$ are presented in

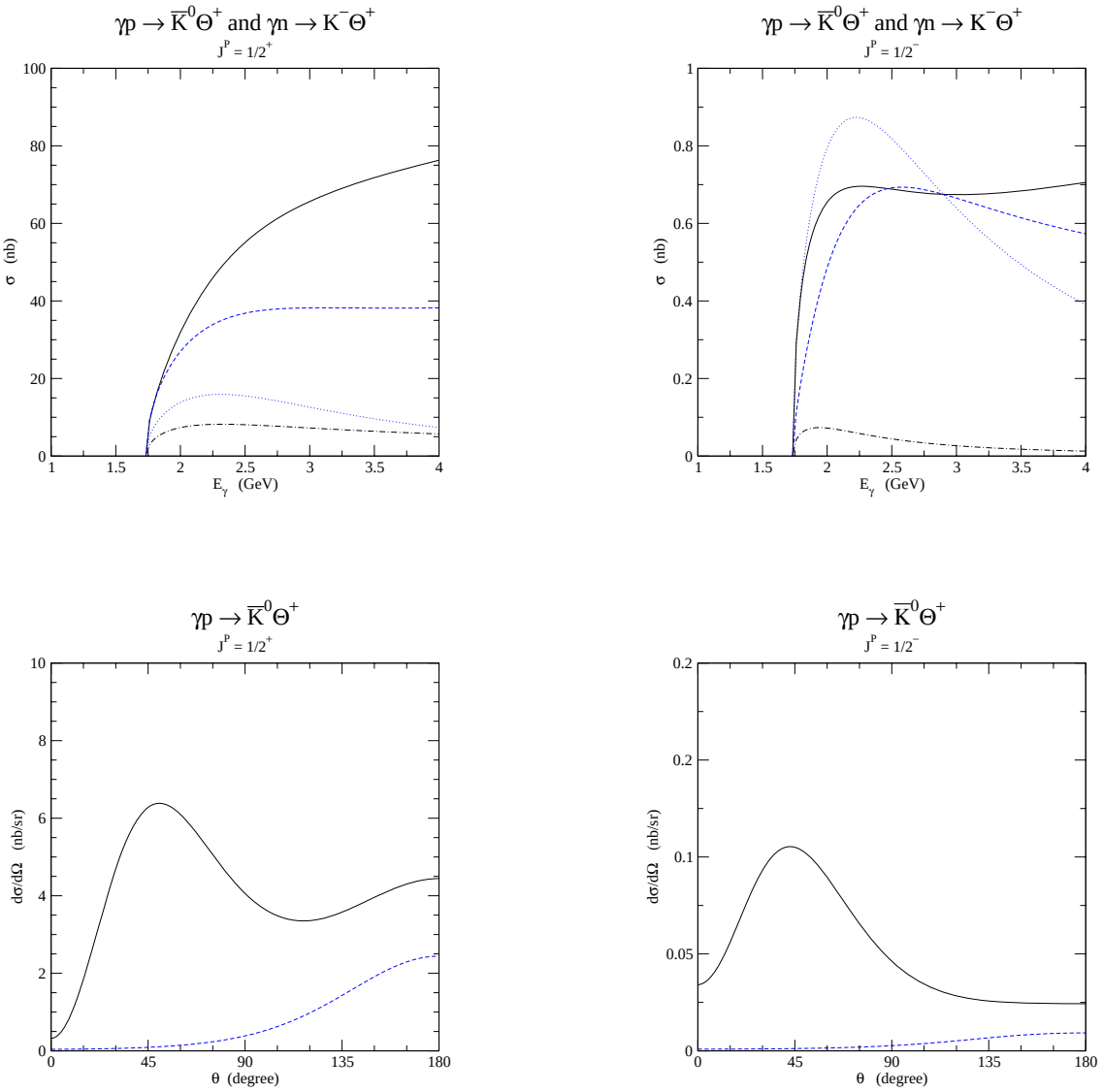

Figure 3: Total cross sections for the positive (upper left panel) and negative (upper right panel) parity Θ^+. Reaction $\gamma p \to \bar{K}^0\Theta^+$: the solid line is with $g_{K^*N\Theta} = g_{KN\Theta}$ and dot-dashed line is with $g_{K^*N\Theta} = 0$. Reaction $\gamma n \to K^-\Theta^+$: the dashed line is with $g_{K^*N\Theta} = g_{KN\Theta}$ and dotted line is with $g_{K^*N\Theta} = 0$. (see details in ref. [31]). Differential cross sections for the positive (lower left panel) and negative (lower right panel) parity Θ^+ for the reaction $\gamma p \to \bar{K}^0\Theta^+$. The solid line is with $g_{K^*N\Theta} = g_{KN\Theta}$ and dashed line is with $g_{K^*N\Theta} = 0$). The scattering angle θ is defined by the directions of the initial photon momentum and the K meson momentum in the CM frame.

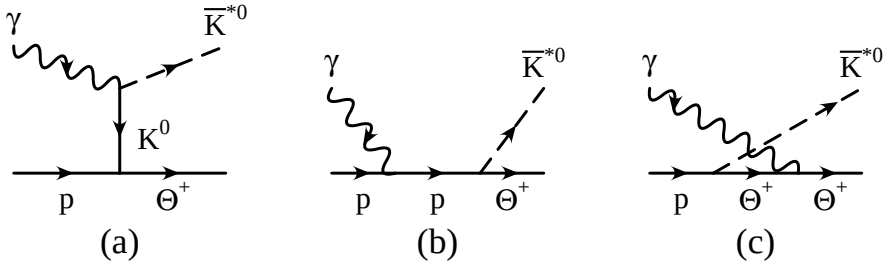

Figure 4: Feynman graphs for possible Θ^+ photo-production from a proton.

Figs. 3. Ref. [33] estimated the $g_{K^*N\Theta}$ coupling constant in the framework of the chiral quark-soliton model and found that the vector meson coupling to the octet-antidecuplet transitions is anomalously small. In the non-relativistic limit this coupling is exactly zero. This can considerably simplify the analysis. From Fig. 3 one can expect that the proton cross section to be a factor of 2 larger or the same order than the neutron cross section and to have a value about 10–70 nb.

The important point is that if the Θ^+ has positive parity, its photoproduction cross section is an order of magnitude larger than if it has negative parity. The calculated differential cross sections are presented in Fig. 3. The angular distributions strongly depend on the production mechanism. In the case where $g_{K^*N\Theta} = 0$ (dotted line) the $\bar{K}^0$ goes backward with respect to the photon beam, while with $g_{K^*N\Theta} = \pm 2.2$ the peak is in the forward direction. Thus, it appears that analysis of the total cross section of the $\gamma p \to \bar{K}^0\Theta^+$ reaction can definitely determine the parity of the Θ^+ baryon, and the production mechanism will manifest itself in the angular distribution.

The Θ^+ production from a proton target in the $\gamma p \to \pi^+ K^- K^+ n$ reaction was first analyzed by CLAS [4, 5]. Two different production mechanisms were explored. While the data seem to suggest one mechanism over the other, the limited statistics prevent a definite conclusion. An estimate of the cross section for Θ^+ production from a proton target in the reaction $\gamma p \to K_0^*\Theta^+$ was made in [34] and [32]. The total cross section for the production of positive and negative parity Θ^+ in the reaction $\sigma(\gamma p \to K_0^*\Theta^+)$ as a function of the photon energy E_γ is presented in Fig. 5. These theoretical estimates of the cross section suggest a search for Θ^+ in the energy region slightly above threshold, i.e. $E_\gamma \sim$ 3-5 GeV. There are two features of these calculations. First of all the theoretical calculations are not very sensitive to the theoretical parameters which makes the cross section estimates more robust. Secondly, the total cross section for the production of negative parity Θ^+ is suppressed by a factor of 10 in comparison with positive parity Θ^+. These two factors make it possible to determine the Θ^+ parity using the value of the total cross section.

2.2 Regge Model

An estimate of the Θ^+ production cross section in the framework of a Regge model was done in [35]. The Regge model predictions for the reaction $\gamma p \to \bar{K}^0\Theta^+$ are presented in Fig. 6 for positive and negative parities of the Θ^+ resonance. The total cross section for negative parity is only a factor of 3 less than for positive parity. The differential cross

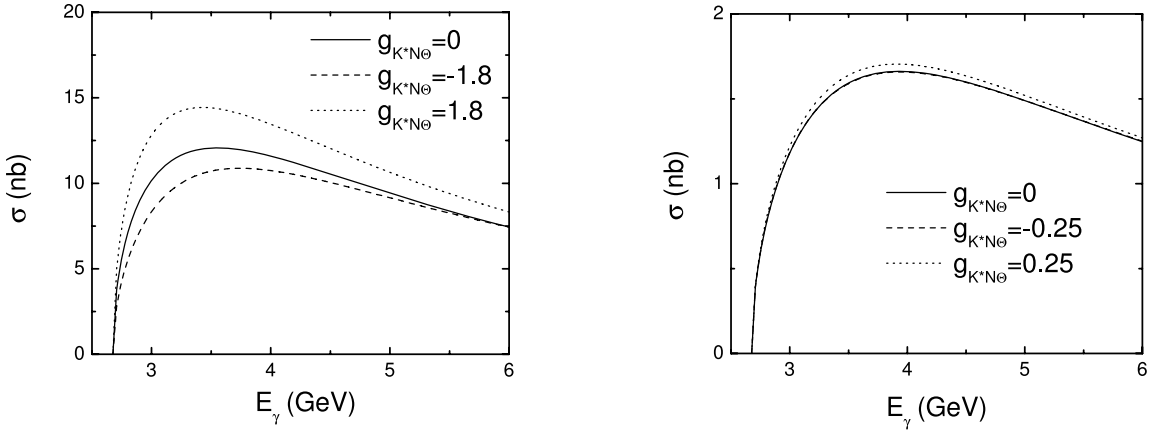

Figure 5: Total cross section for the production of positive (left panel) and negative (right panel) parity Θ^+ in the reaction $\gamma p \to \pi^+ K^- \Theta^+$ as a function of photon energy for the different values of the coupling constant $g_{K^* N \Theta}$.

section shows different behavior for different production mechanisms.

The photon asymmetry is found to display a pronounced sensitivity to the parity of the Θ^+, making it a very promising observable to help determining the quantum numbers of this particle. It opens the possibility to determine the parity in experiments with polarized electron beams.

The total and differential cross section for the reaction $\gamma p \to K_0^* \Theta^+$ is presented in Fig. 7. In this case the ratio of the positive to negative parity cross section is of the order of 10.

3 Analysis of prior CLAS data, and the issue of Reaction Mechanism.

The CLAS data used in the analysis which lead to the observation of the Θ^+ photoproduced from the proton came fron the three g6 running periods (*a*,*b*, and *c*). In addition to unequivocally observing the state in several different running periods involving very different experimental conditions, the two methods of analysis yielded some interesting questions about the production mechanism. These will be described below. The first analysis, denoted *Analysis I*, was based on the assumption that the Θ^+ is produced by a kaon $t-channel$ process illustrated in Fig. 4 a. The second, denoted *Analysis II*, was based on the assumption that the Θ^+ is produced by a $t-channel$ process which produces a leading

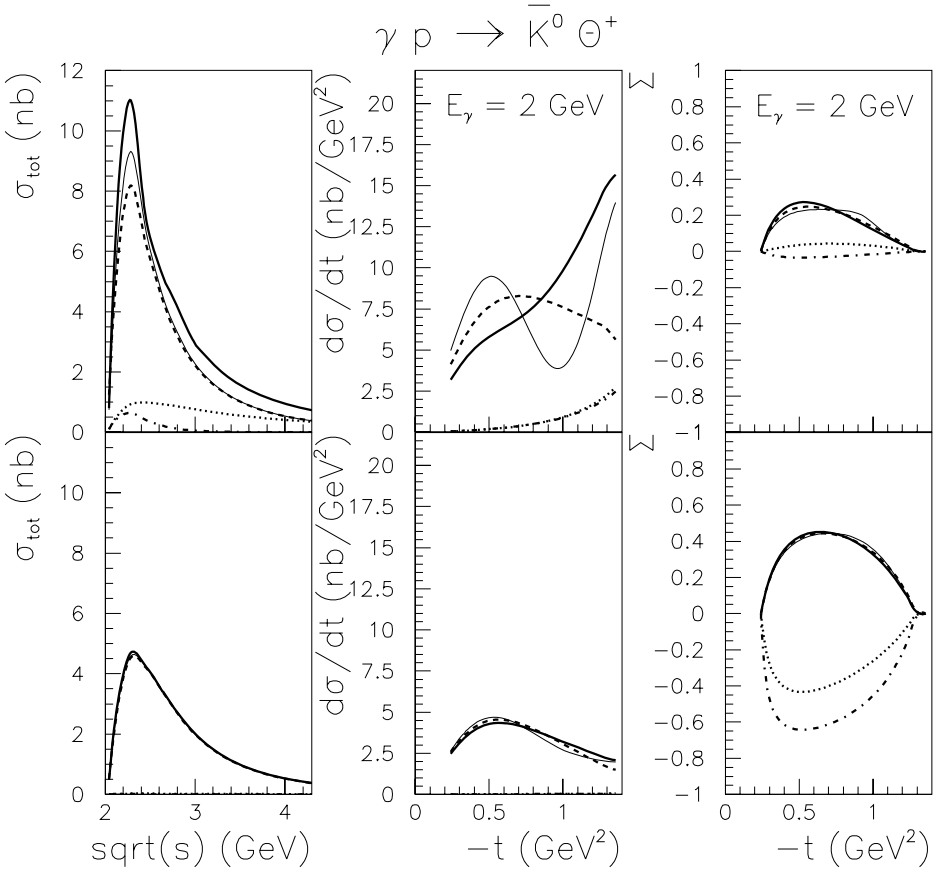

Figure 6: Regge model predictions for the $\gamma p \to \bar{K}^0\Theta^+$ reaction for both possible parities of the Θ^+. Upper panels: positive parity; lower panels: negative parity. left panel: total cross section; middle panel: differential cross section; right panels: photon asymmetry. Dashed curves: K^* Regge exchange; dashed-dotted curves: gauge-invariant $s+u$ channel exchange; thin solid curves: sum of K^* $s+u$ reggeized exchange. For comparison, the results are also shown when using the pole exchange for the $s+u$ channel processes. $s+u$ pole exchange (dotted curves); sum of reggeized K^* exchange, and $s+u$ pole exchanges (thin solid curves).

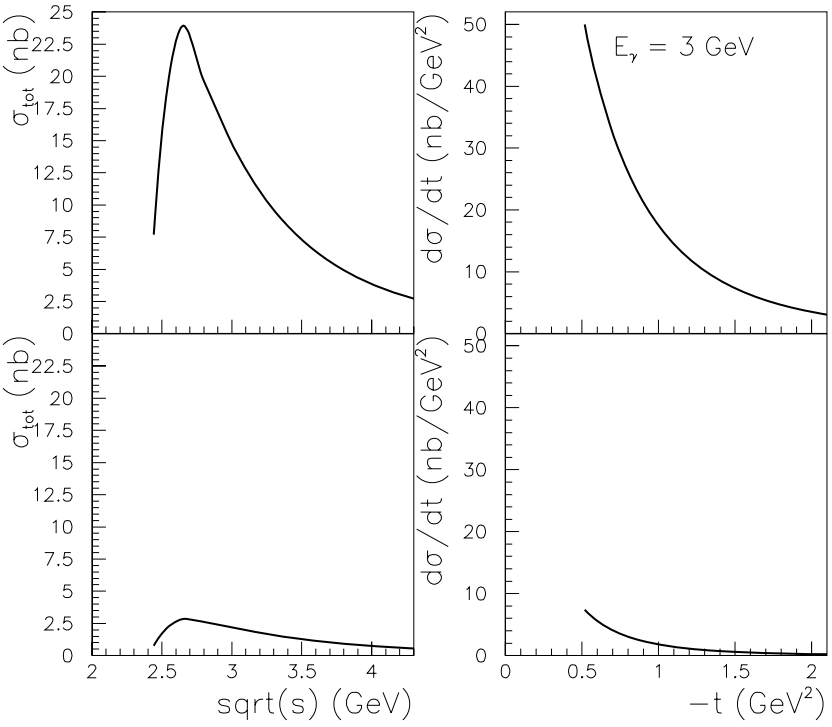

Figure 7: Regge model predictions for the $\gamma p \to \bar{K}_0^* \Theta^+$ reaction for both possible parities of the Θ^+. Upper panels: positive parity; lower panels: negative parity. The curves correspond with K^* Regge exchange.

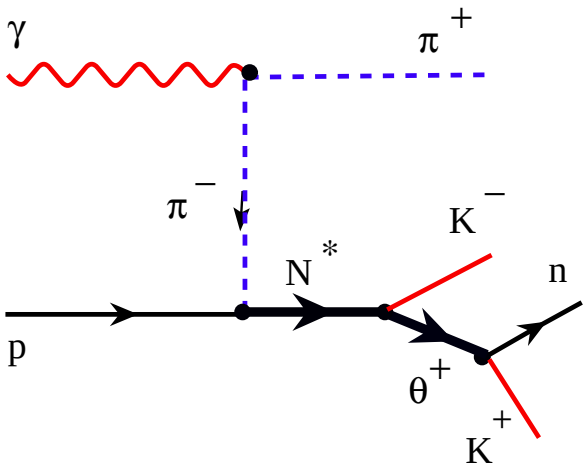

Figure 8: Feynman graphs for possible Θ^+ photo-production from a proton.

π^-, illustrated in Fig. 8.

3.0.1 Analysis I: kaon t-channel process.

For this analysis, data from the g6a and g6b run periods were used. Events were selected with a positive pion and two kaons of opposite sign in the final state.

Fig. 9 shows the angular distribution of the $K^-\pi^+$ system versus the invariant mass in the reaction $\gamma p \to \pi^+ K^- K^+ n$. Note the peak corresponding to the $K^{*0} \to K^-\pi^+$ decay. In order to select the kaon $t-channel$ process only events with $cos\theta_{K^-\pi^+} > 0.5$ were selected (the angle $\theta_{\pi^+ K^-}$ is between the $\pi^+ K^-$ system and photon beam in the center of mass). This cut is driven by the theoretical hypothesis of t-channel Θ^+ production from a proton. The $K^+ n$ invariant mass distribution in the reaction $\gamma p \to \pi^+ K^- K^+ n$ is shown in Fig. 10. The resulting fit yields 31 counts in the peak with the mass $M = 1.556$ GeV/c^2 and width $\sigma = 8$ MeV/c^2. The mass scale uncertainty is estimated as $\pm$ 10 MeV/c^2. This uncertainty is mainly due to the energy calibration of the CLAS detector. The mass resolution is close to the experimental resolution of CLAS as can be seen from the various distributions in this document.

3.0.2 Analysis II: pion t-channel process.

For this case the data used in *Analysis I* above was augmented by including data from three distinct data runs with different running conditions in CLAS, including the analysis of the reactions $\gamma p \to \pi^+ K^+ K^- n$ and $\gamma p \to K^+ K^- p$. Two data runs, g6a and g6b, used in *Analysis I*, had identical geometrical acceptance and trigger conditions, but different beam energies. Run g6a had a photon beam energy range 3.2–4.0 GeV, run g6b 3–5.3 GeV.

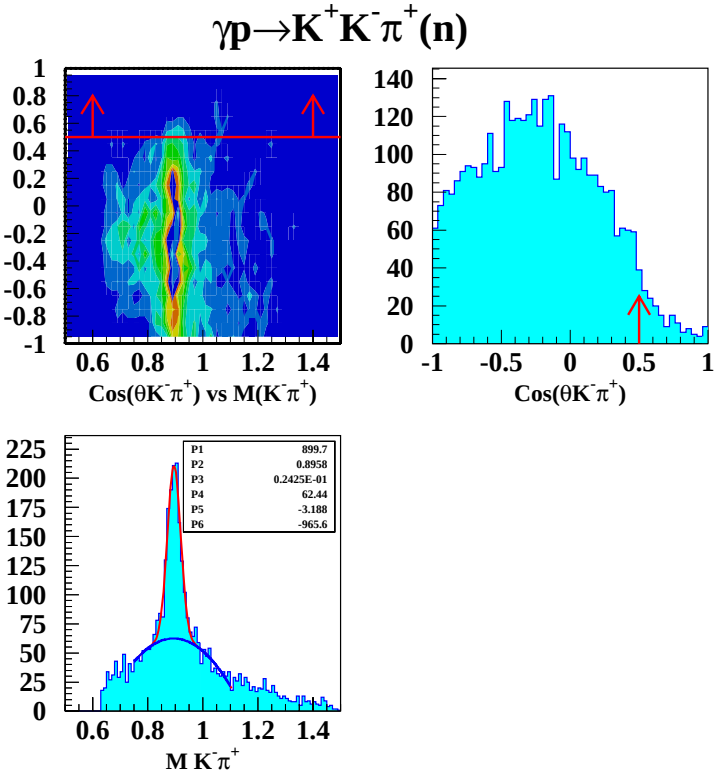

Figure 9: The reaction $\gamma p \to \pi^+ K^- K^+(n)$. The neutron was identified by the missing mass technique. a) Scatter plot of $cos\theta_{K^-\pi^+}$ vs $K^-\pi^+$ invariant mass. b) The $cos\theta_{K^-\pi^+}$ distribution for all events. c) The $K^-\pi^+$ invariant mass distribution, where the K^{0*} peak is clearly seen. Here, $\theta_{K^-\pi^+}$ is the angles between the $K^-\pi^+$ system and photon beam in the center of mass. The arrows indicate the cut $cos\theta_{K^-\pi^+} > 0.5$ that was applied for selection of Θ^+ candidates.

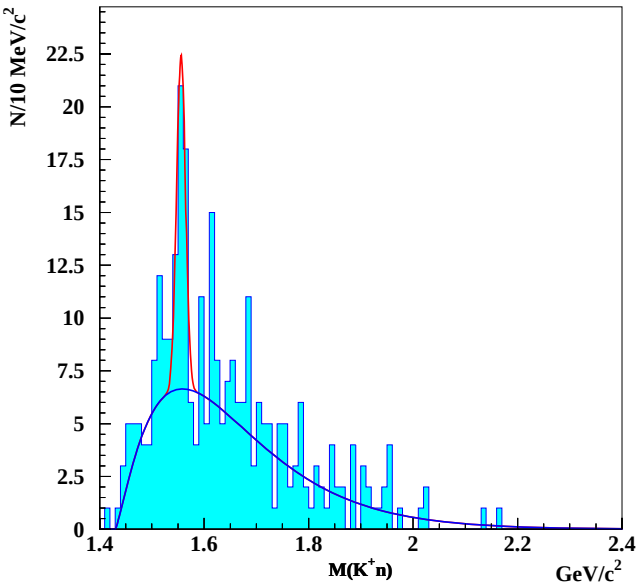

Figure 10: The K^+n invariant mass distribution in the reaction $\gamma p \to \pi^+ K^- K^+ n$.

Data from a third run, g6c, with energy 4.8–5.5 GeV, and having very different geometry, acceptances, and trigger conditions than g6a and g6b was also analyzed. The estimated combined g6a and g6b integrated luminosity is about 2 events/pb, and run g6c has about 2.7 events/pb. The final nK^+ invariant mass spectrum calculated from the missing mass in the reaction $\gamma p \to \pi^+ K^- K^+ n$, combining data from all three data runs, is shown in Fig. 11.

To enhance the pion *t-channel*, two angular cuts in the center of mass system were applied to extract the signal and suppress the background. The structure in the region of 1.55 GeV/c^2 appears after cutting $cos\theta^*_{\pi^+} > 0.8$, where $\theta^*_{\pi^+}$ is the center-of-mass angle between the π^+ and the photon beam. This cut approximately corresponds to $-t < 0.28$ GeV/c^2 in our beam energy range, where $t = (k - p)^2$, k is the photon 4-momentum, and p is the pion 4-momentum. The reaction $\gamma p \to \pi^+ K^- K^+ n$ is dominated by meson resonance production decaying to $K^+K^-\pi^+$ with small momentum transfer to the proton, and the excitation of baryon resonances decaying to $n\pi^+$ or nK^-. These processes have the K^+ moving forward in the center of mass system. To suppress such backgrounds, a cut was applied to select events having a positive kaon going in the backward direction with $cos\theta^*_K < 0.6$. The Θ^+ peak was clearly observed in each of the three data sets; the resulting nK^+ mass spectrum were combined and are shown in Fig. 12.

The nK^+ effective mass distribution was fitted by the sum of a Gaussian function and a background function obtained from phase space simulation. The fit parameters are: $N_{\Theta^+} = 41 \pm 10$, $M = 1555 \pm 1$ MeV/c^2, and $\Gamma = 26 \pm 7$ MeV/c^2 (FWHM). The mass

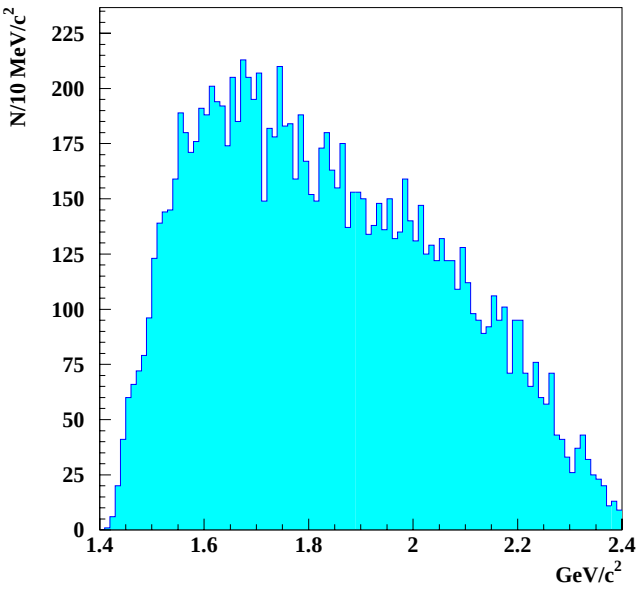

Figure 11: The M_{nK^+} invariant mass spectrum in the reaction $\gamma p \to \pi^+ K^- K^+ (n)$. The neutron was identified by the missing mass technique.

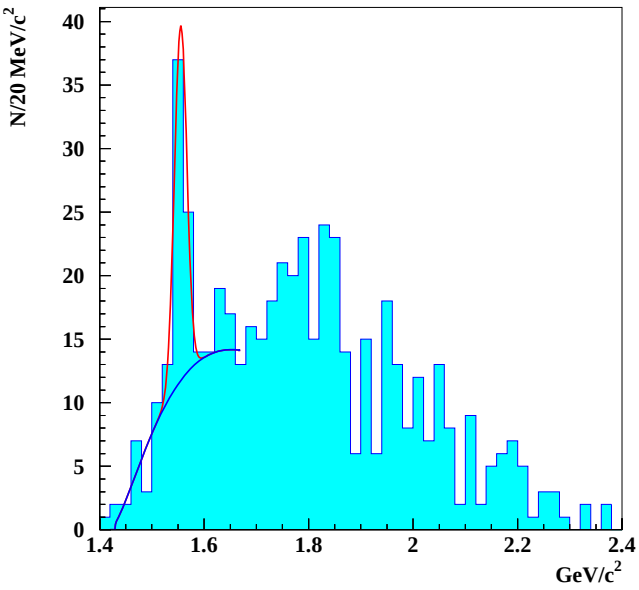

Figure 12: The K^+n invariant mass spectrum in the reaction $\gamma p \to \pi^+K^-K^+(n)$ with the cut $cos\theta^*_{\pi^+} > 0.8$ and $cos\theta^*_{K^+} < 0.6$. $\theta^*_{\pi^+}$ and $\theta^*_{K^+}$ are the angles between the π^+ and K^+ mesons and photon beam in the center of mass system. The background function we used in the fit was obtained from a phase space simulation.

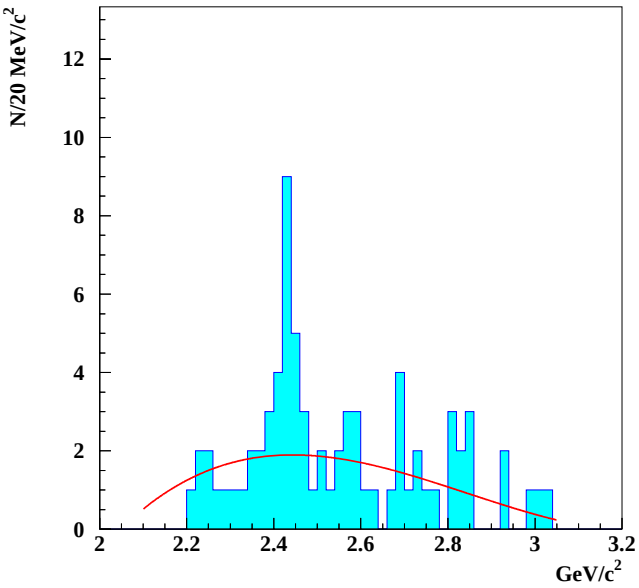

Figure 13: The $M_{nK^+K^-}$ invariant mass spectrum calculated from the missing mass off of the π^+ in the reaction $\gamma p \to \pi^+ K^- K^+(n)$ with the cuts $cos\theta^*_{\pi^+} > 0.8$ and $cos\theta^*_{K^+} < 0.6$. $\theta^*_{\pi^+}$ and $\theta^*_{K^+}$ are the angles between the π^+ and K^+ mesons and photon beam in the center of mass system. The events in this plot have $M(K^+n)$ between 1.54 and 1.58 GeV/c^2. The shape of the background curve was obtained from our phase space simulation.

scale uncertainty is estimated to be ± 10 MeV/c^2. This uncertainty is mainly due to the momentum calibration of the CLAS detector and the photon beam energy calibration. The statistical significance of the fit in Fig. 12 calculated over a 40 MeV/c^2 mass window is 7.8 σ. The fact that the angular cuts we applied enhanced the Θ^+ signal suggests the possible production of a N^*/Δ^* that decays to Θ^+ and K^-. If the Θ^+ is an isosinglet, the intermediate state can only be an N^*. For the events with nK^+ effective mass between 1.54 and 1.58 GeV/c^2, the missing mass off of the π^+ is shown in Fig. 13. The apparent excess of events near 2.4 GeV/c^2 are suggestive of an intermediate baryon state. The simulation that we have completed using phase space confirmed that the angular cuts we applied cannot generate narrow peaks in either the nK^+ or the nK^+K^- effective mass spectrum.

While exploring these various t-channel processes, some puzzles appeared which need to be resolved. For example, although the Θ^+ appeared to be associated with *t-channel* $K^-\pi^+$ production in runs g6a and g6b, this was not found to be evident in the g6c run. On the other hand, the pion *t-channel* process may be consistent all three data sets. We studied the Θ^+ association with $\bar{K}^*_0$ by cutting on the $K^-\pi^+$ invariant mass around the $\bar{K}^*_0$. The $K^-\pi^+$ invariant mass shows a clear $\bar{K}^*_0$ signal (Fig. 14) in the final data sample that produced Fig. 12. The results are shown in Fig. 15, and suggests that the Θ^+ is not

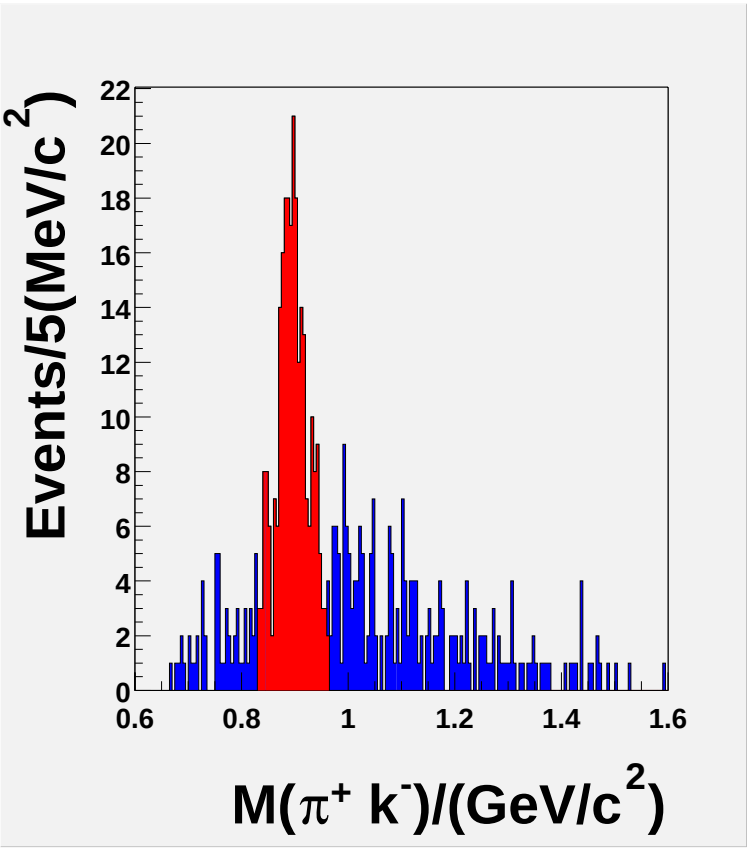

Figure 14: The $K^-\pi^+$ invariant mass spectrum for the events that went into the plot in Fig. 12 in the reaction $\gamma p \to \pi^+ K^- K^+(n)$ with the cuts $cos\theta^*_{\pi^+} > 0.8$ and $cos\theta^*_{K^+} < 0.6$. $\theta^*_{\pi^+}$ and $\theta^*_{K^+}$ are the angles between the π^+ and K^+ mesons and photon beam in the center of mass system. The $\bar{K}^*_0$ signal is clearly visible.

strongly associated with the $\bar{K}^*_0$.

We note that g6a and g6b, and g6c, were run in two different experimental configurations. While g6a and g6b ran with the target in the nominal position, and full torus field to maximize resolution, g6c ran with the target displaced upstream by 1m and had low torus field, to maximize forward acceptance.

This issue could have a fundamental implication in terms of the nature of the Θ^+ particle. For example, if Θ^+ is indeed an isotensor, as suggested in [36], then the exchange of K^0 to produce a Θ^+ at the bottom vertex and a $\bar{K}^*_0$ at the meson vertex (Fig. 4 a) is forbidden by isospin conservation.

In any case, this puzzle needs to be resolved. Higher statistics over a wide energy range is essential to clarify this issue. No matter what is the reason behind such observation in terms of the production mechanism, more data is certainty needed to investigate this issue.

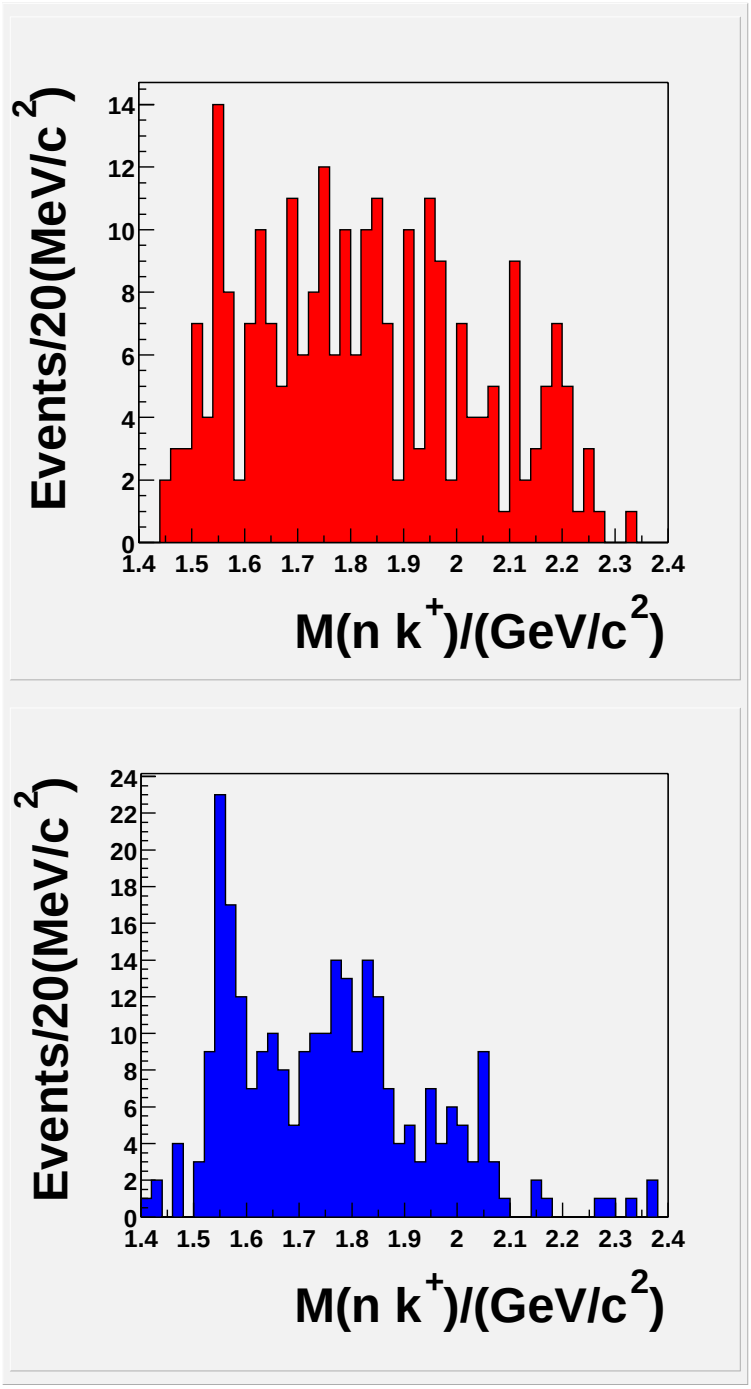

Figure 15: The nK^+ invariant mass spectra in the reaction $\gamma p \to \pi^+ K^- K^+(n)$ with the cuts $cos\theta^*_{\pi^+} > 0.8$ and $cos\theta^*_{K^+} < 0.6$. The top plot in red is for the events with $K^-\pi^+$ invariant mass around the $\bar{K}^*_0$. The bottom plot in blue is associated with the non-$\bar{K}^*_0$ events. The data suggests that the Θ^+ is at best only weakly produced in association with $\bar{K}^*_0$, and possibly not at all.

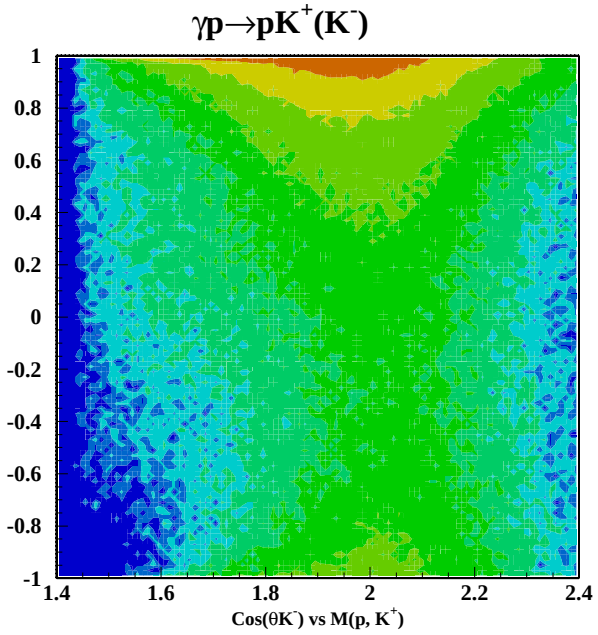

Figure 16: The $dN/dcos\theta_{K^-}$ vs M_{pK^+} invariant mass distribution in the center of mass system in the reaction $\gamma p \to pK^+ + (K^-)$. The K^- was identified by missing mass.

4 Search for X^{++} in the reaction $\gamma p \to K^- X^{++}, X^{++} \to pK^+$

More than 200K events with a proton and positive kaon in the final state were selected for this analysis. The K^- was identified by the missing mass technique. The scatter plot $dN/dcos\theta_{K^-}$ vs M_{pK^+} in the center of mass system in the reaction $\gamma p \to pK^+ + (K^-)$ is presented in Fig. 16. The K^- is moving predominantly in the forward direction in the center of mass system. No obvious structures in the M_{pK^+} invariant mass spectrum are observed in this plot. The M_{pK^+} distribution is presented in Fig. 17. Note that no resonance peaks are apparent; Θ^{++} cross sections however are completely unknown, and more data will increase the statistical significance of this result.

5 Spin-parity

Without some model of the production mechanism of the Θ^+ there is almost no possibility of directly measuring the spin or parity. However, we may anticipate that an experimental run that produces a reasonable number of events may give sufficient information on reaction dynamics to make a spin-parity determination.

As an example, let us consider the reaction mechanism suggested by the g6 analysis, that is the production through a t-channel process of an intermediate nucleon resonance. If this is correct, it may be possible to form this state through the s-channel as shown in Fig. 18.

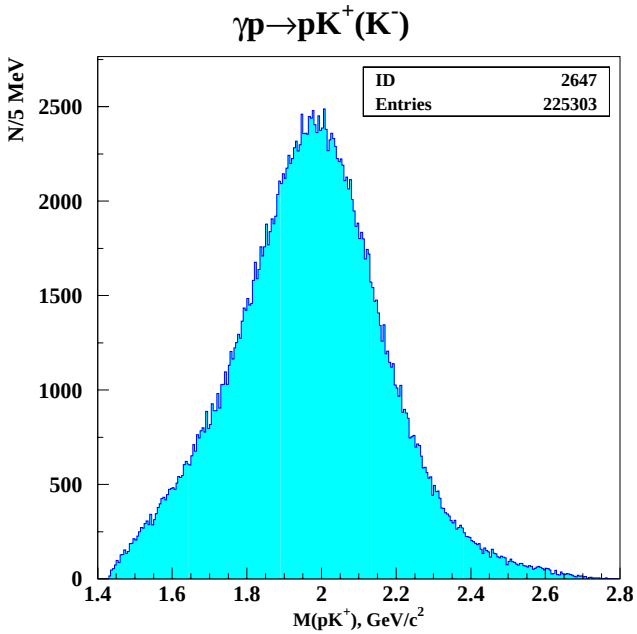

Figure 17: The M_{pK^+} invariant mass distributions in the reaction $\gamma p \to pK^+(K^-)$. The K^- was identified by missing mass.

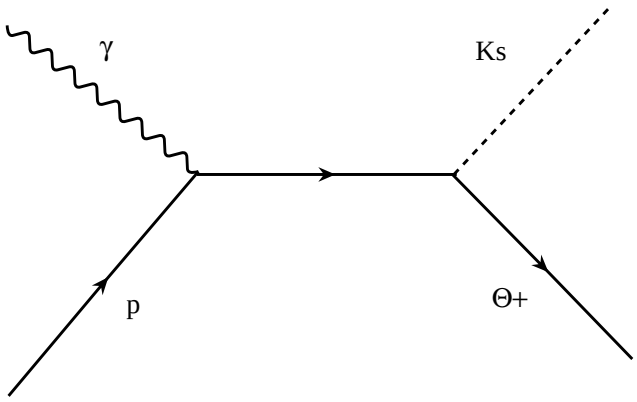

Figure 18: Possible Feynman diagram for the production of the Θ^+ via an intermediate N^* state.

If the spin-parity of the initial state is known, an analysis of the angular distribution of the Θ^+ can determine the spin-parity of the Θ^+. For example, in Fig. 19 we show the angular distributions of the decay $\Theta^+ \to nK^+$ for both hypothesis $J^P_{\Theta^+} = \frac{1}{2}^+$ and $\frac{3}{2}^+$ for the decay of a $\frac{5}{2}^+$ resonance produced in an $M = \frac{1}{2}$ state.

If the J^P of the intermediate N^+ is not known, which of course is likely, a fit to the total angular distribution may be performed to determine the spin-parities of both states.

Finally, the same technique may be generalized to the t-channel production of the intermediate N^*. In fact, if the production of the resonance is due to the exchange of a spinless meson, the analysis may even be simpler.

As an example of the expected statistical significance of this planned experimental run, simulated data with the expected number of signal Θ^+ events together with the appropriate background was generated. The reaction for the signal was the t-channel production of a high mass N^* state decaying to $\Theta^+ K^-$, with a π^+ going foward in the center-of-mass with an exponential t slope of 5 GeV^{-2}. The beam energy was 5 GeV exactly simulating g6c conditions. The background events were simulated from the results of a partial wave analysis of the reaction $\gamma p \to K^+ K^- \pi^+ n$, which accurately describes the majority of the background events.

The results of the analysis are shown in Fig. 20. The meson background events were subtracted from the momentum transfer distribution to the π^+ and fitted to an exponential distribution. The fitted slope was 5.7 GeV^{-2}, which is a measure of the statistical sensitivity of the proposed experimental run, for this particular beam energy range. In the actual

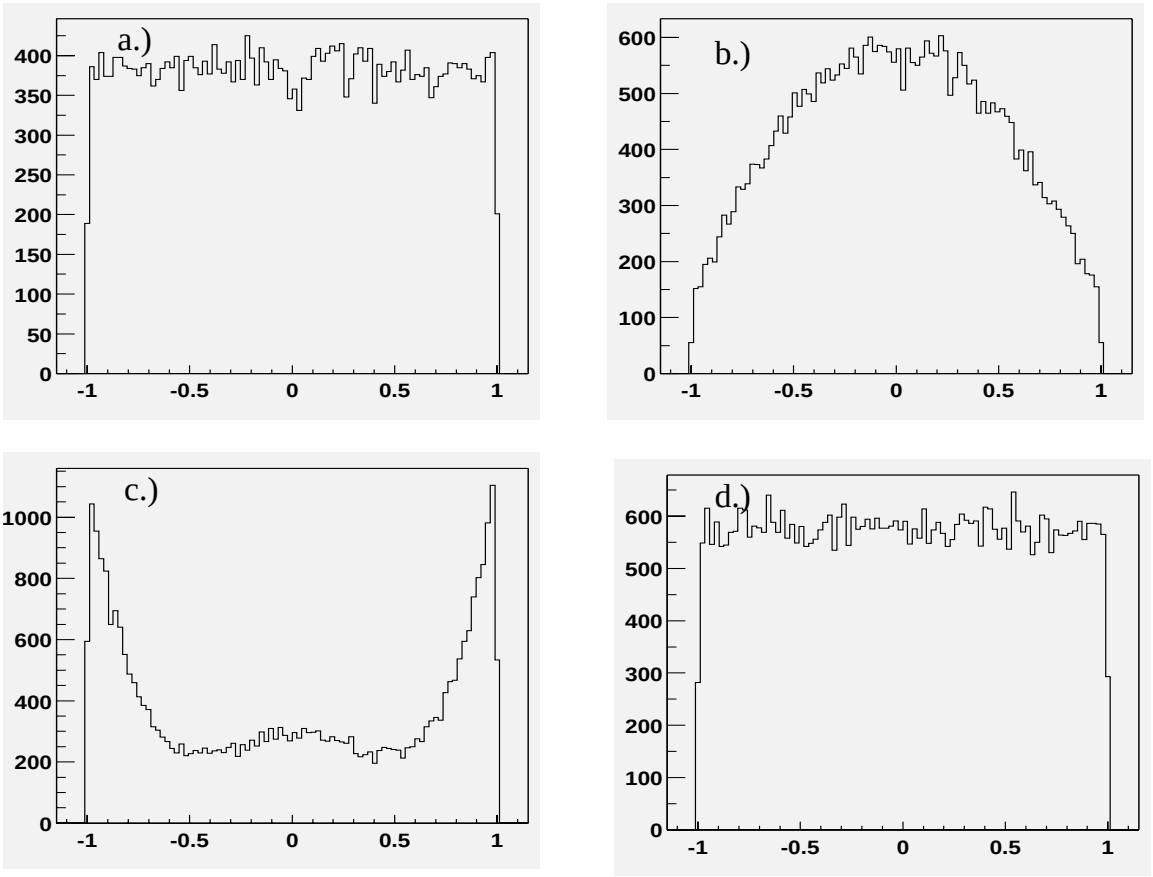

Figure 19: Decay angular distributions of a D_{15} N* resonance formed (s-channel) in an $M = \frac{1}{2}$ state, decaying into $\Theta^+ K_s$. The Θ^+ subsequently decays into nK^+. a.) $cos(\theta)$ of the K^+ in the helicity frame of the Θ^+ for $J^P = \frac{1}{2}^+$. b.) $cos(\theta)$ of the K^+ in the helicity frame of the Θ^+ for $J^P = \frac{3}{2}^+$. c.) $cos(\theta)$ of the K_s in the center-of-mass for case (a) above. d.) $cos(\theta)$ of the K^+ in the helicity frame of the Θ^+ for $J^P = \frac{1}{2}^-$.

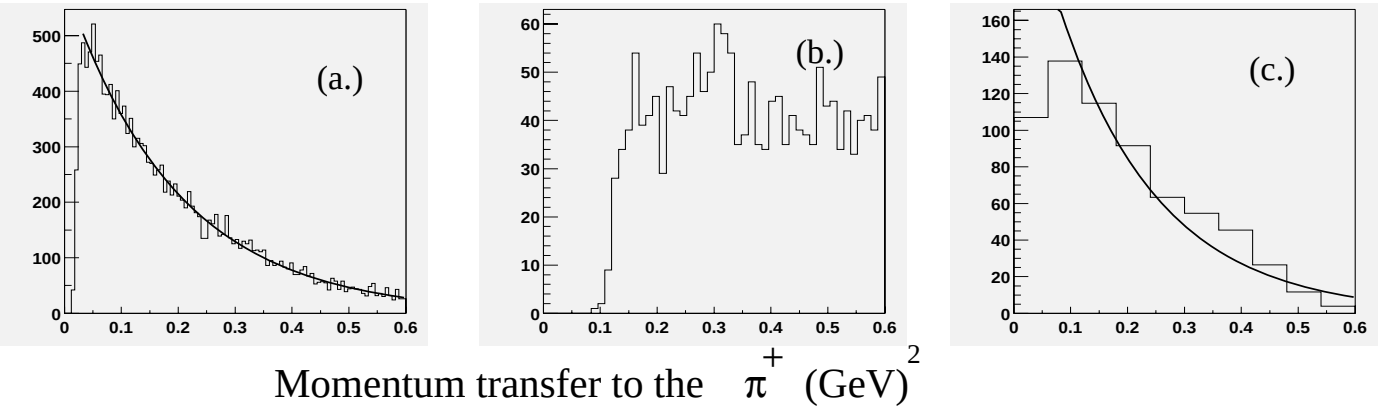

Figure 20: The results of simulated study of the Θ^+ production mechanism from the reaction $\gamma p \to \pi^+ N^*(2400)$, $N* \to \Theta^+ K^-$, $\Theta^+ \to nK^+$ with expected signal and background from t-channel meson production in a 40 day run. (a) Generated momentum transfer to the π^+ for the N^* events; the exponential slope was 5 GeV^{-2}. (b) Momentum transfer to the π^+ for the meson background events. (c) Background subtracted momentum transfer distribution (with the correct expected statistics) The fitted exponential slope is 5.7 GeV^{-2}.

experiment, we will have data on the Θ^+ from threshold to the highest photon energies available.

We have also simulated the reaction $\gamma p \to \pi^+ K^+ K^- n$ with two sets of included events: an N*(2400) produced in a t-channel process with a foward π^+, and meson background events with the correct angular distributions measured by a partial wave analysis in g6c. The N* then decays to $\Theta^+ K^-$, where the J^P of the Θ^+ is $\frac{3}{2}^+$. Shown in Fig. 21 is $cos(\theta_{helicity})$ of the K^+ in the nK^+ helicity frame for both the background events, which can be subtracted, and the total simulated event sample.

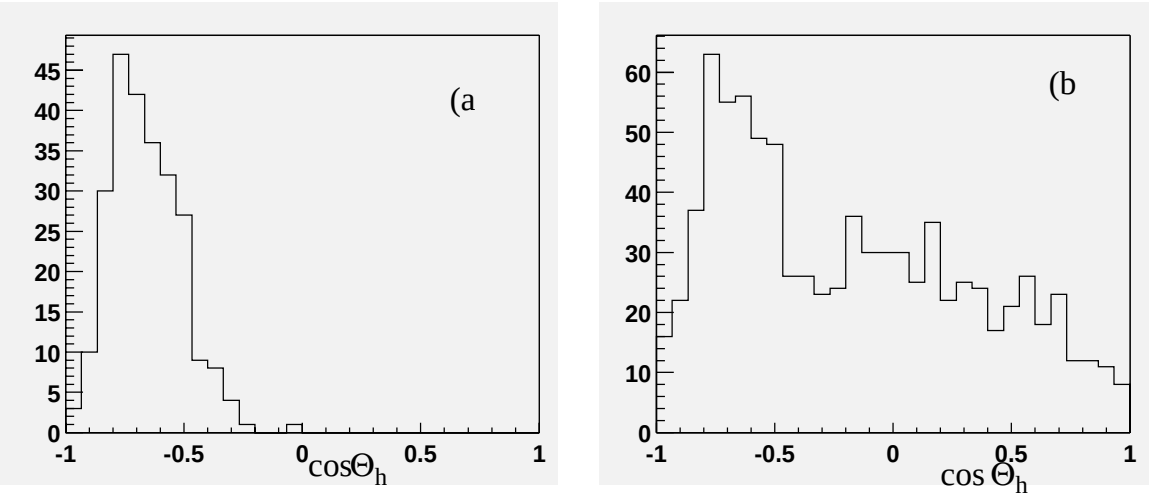

Figure 21: Decay angular distributions of a D_{15} N* resonance produced in a t -channel process with a foward π^+. The N* is in an $M = \frac{1}{2}$ state, decaying into $\Theta^+ K^-$, where the J^P of the Θ^+ is $\frac{3}{2}^+$. The Θ^+ subsequently decays into nK^+. The statistics is the expected event count from a 40 day run including meson background events. a.) $cos(\theta)$ of the K^+ in the helicity frame of the nK^+ of the meson background events. b.) $cos(\theta)$ of the K^+ in the helicity frame of the nK^+ for all events.

Part II
Cascade Physics and the Search for the Ξ_5

1 Introduction

The Ξ_5 is the cascade member of the pentaquark antidecuplet. It consists of four charge states: Ξ_5^{--}, Ξ_5^-, Ξ_5^0, and Ξ_5^+. NA49 claims to have seen two of these charge states, the Ξ_5^{--} and the Ξ_5^0, of this particle at a mass of 1862 MeV [37]. Confirming the existence of this state, and the determination of its properties, are critically important to understanding the nature of the pentaquarks. The only calculation of the cross section for the production of this particle to date has been made by Liu [38], who used an SU(3) hadronic model with a U(1) photon gauge particle to calculate the cross sections for $\gamma p \to K^0 K^0 \Xi_5^+$ and $\gamma n \to K^+ K^+ \Xi_5^{--}$.

The Ξ_5 may be detected in photoproduction off the proton in any of several processes. These are listed in Table 1 for the processes most likely to find an unambiguous signal. For instance, we do not list the process $\gamma p \to K^0 K^0 \Xi_5^+$, since the nature of the K^0 strangeness makes it impossible to determine the strangeness of the final state baryon. Note that all Θ^+ results which identify the Θ^+ in the $K_s^0 p$ invariant mass conclude that the peak they find corresponds to a pentaquark because there are no known Σ^* states in the mass region of 1540 MeV.

Table 1: Photoproduction reactions to produce the Ξ_5 using a proton target.

Reaction	Threshold (GeV)
$\gamma p \to K^+K^+\pi^+\Xi_5^{--}$	4.3
$\gamma p \to K^+K^+\Xi_5^-$	3.9
$\gamma p \to K^+K^+\pi^-\Xi_5^0$	4.3
$\gamma p \to K^+K^+\pi^-\pi^-\Xi_5^+$	4.7

2 Results from existing data

The *g6a*, *g6b*, and *g6c* data sets have all been studied to look for Ξ^- photoproduction. Additionally, we have searched for the Ξ_5^{--} in the *g6b* and *g6c* data sets. Fig. 22 shows the missing mass in the process $\gamma p \to K^+K^+X$ for the *g6a* data set. This figure illustrates the quality we can obtain in the missing mass peak with good particle ID.

Fig. 23 shows a similar missing mass from the g6b data set. In this data set, momentum and energy loss corrections have not yet been applied, so the peak corresponding to the ground state Ξ actually appears about 5–10 MeV low. Also, the particle ID cuts are not set as tightly as in g6a. A result of this is that the event sample is partially contaminated by a background due to π/K misidentification. This is seen in the small peak near 1100 MeV in Fig. 23. Such a peak exhibits a kinematic dependence, and is a reflection of the process $\gamma p \to K^+\pi^+\Sigma^-$. The signal of the $\Xi(1320)$, however, shows no such kinematic dependence.

The g6c data set is our highest energy and highest statistics data set. It consists of approximately $2.7 pb^{-1}$ of γp data in the energy range $4.8 - 5.4$ GeV. Fig. 24 shows the missing mass of the $\gamma p \to K^+K^+X$ reaction from this data set. Because the data were taken at such a high beam flux, we were not able to do a clean π/K separation, which led to a large background. Additionally, we were not always able to correctly identify the photon responsible for the event. We were able to partially recover from this situation by looking at the decay products of the photoproduced Ξ^-. If a π^+ misidentified as a K^+, the event is actually $\gamma p \to K^+\pi^+\Sigma^-$; if both K^+'s are actually π^+, the reaction is $\gamma p \to \pi^+\pi^+\Delta^-$. Neither of these backgrounds will produce a proton in the final state; both the Σ^- and the Δ^- decay nearly 100% of the time to $\pi^- n$. By contrast, the Ξ^- decays roughly 2/3 of the time to $\pi^-\pi^- p$. Fig. 25 shows the same missing mass plot when we require that a proton is also present in the event.

There is a great deal of structure in this plot above the mass of the first excited state at 1530 MeV. Interestingly, every state in the Particle Data Book matches up with an enhancement in the plot, lending credence to the conclusion that these states have been seen. Additionally, there are two structures in the plot that do not appear in the Particle Data Book, at 1770 and 1860 MeV. The structure at 1860 is especially tantalizing; if it is correct, it helps to confirm the NA49 result. We are still analyzing these data, in an attempt to improve the background suppression of this plot.

We may make a first search for the $\Xi_5^{--}(1862)$ in the *g6b* and *g6c* data sets, by looking for the reaction $\gamma p \to K^+K^+\pi^+X$. Fig. 26 shows the *g6b* result for this search, and Fig. 27 shows the *g6c* result.

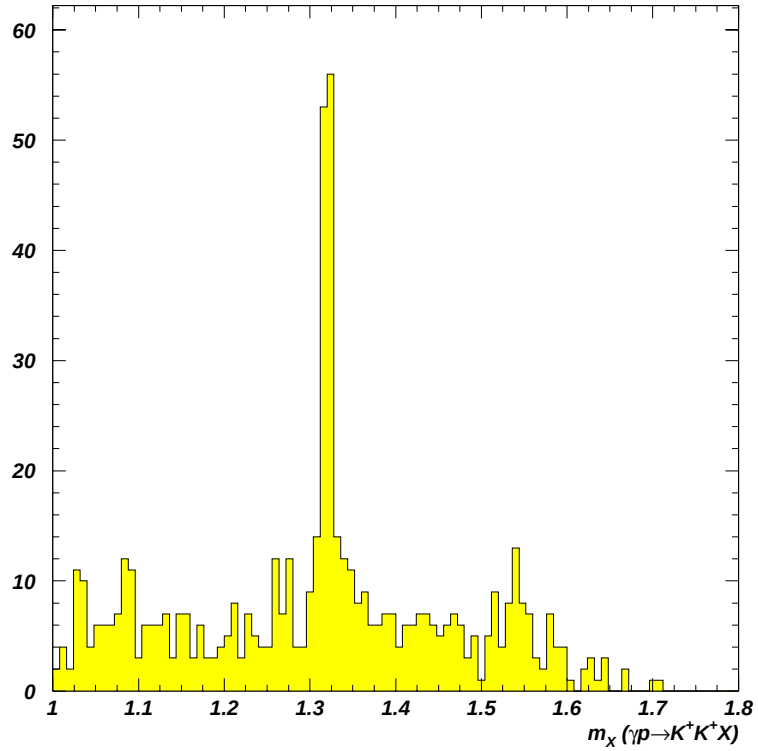

Figure 22: The missing mass in the process $\gamma p \to K^+K^+X$ from the *g6a* data set. The K^+ particle ID has been tightened to enhance the signal of the $\Xi^-(1530)$.

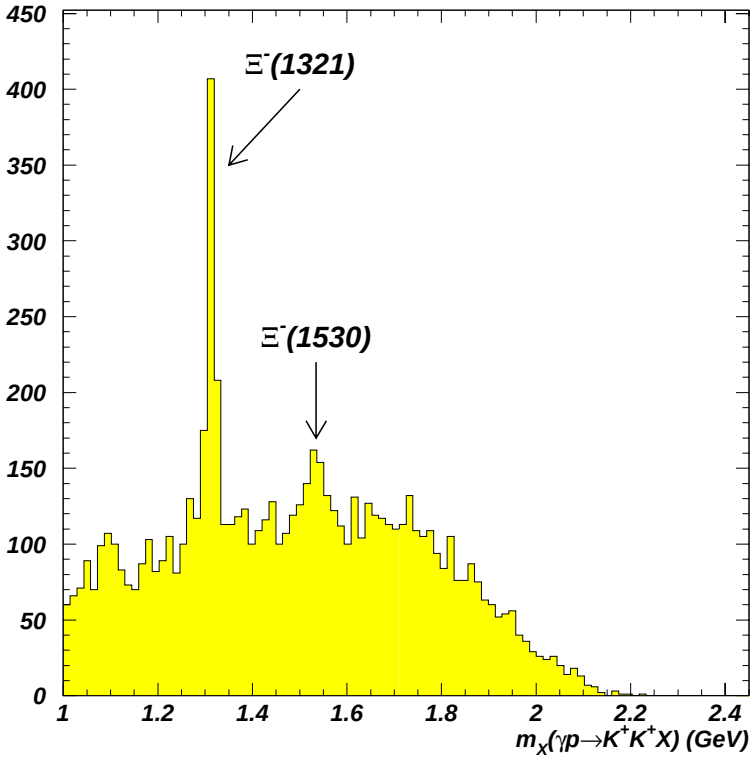

Figure 23: The missing mass in the process $\gamma p \to K^+K^+X$ from the *g6b* data set. Both the ground state $\Xi^-(1321)$ and the first excited state $\Xi^-(1530)$ are clearly seen in the plot. Looser particle ID than in Fig. 22 also introduces a reflection from the process $\gamma p \to K^+\pi^+\Sigma^-$ at 1.1 GeV. The mass is calculated incorrectly due to the π/K misidentification.

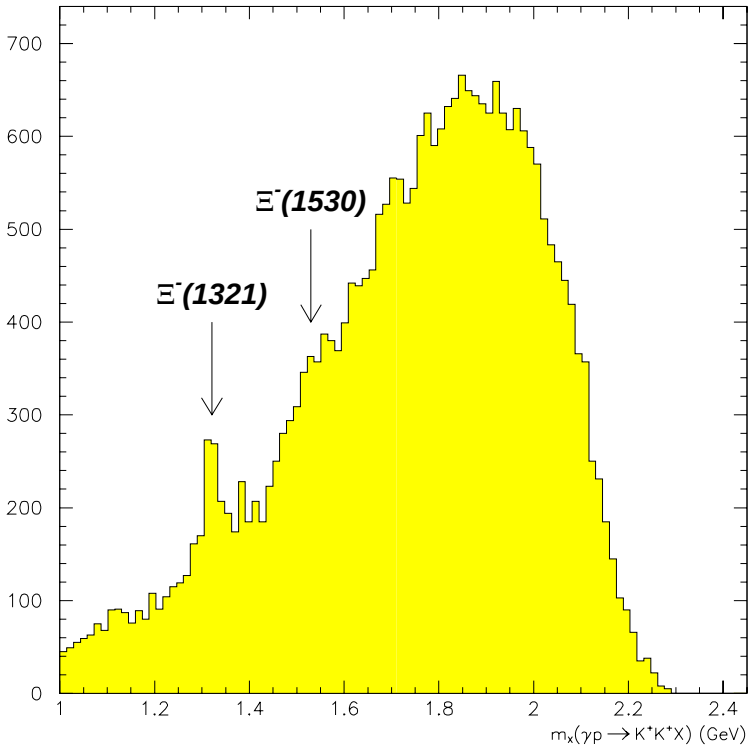

Figure 24: The missing mass in $\gamma p \to K^+K^+X$ data set. Because of the very high beam flux, the particle ID was poor. Only the ground state is clearly seen; the first excited state $\Xi^-(1530)$ appears only as a shoulder in the plot. Higher-mass structure cannot be separated from the background.

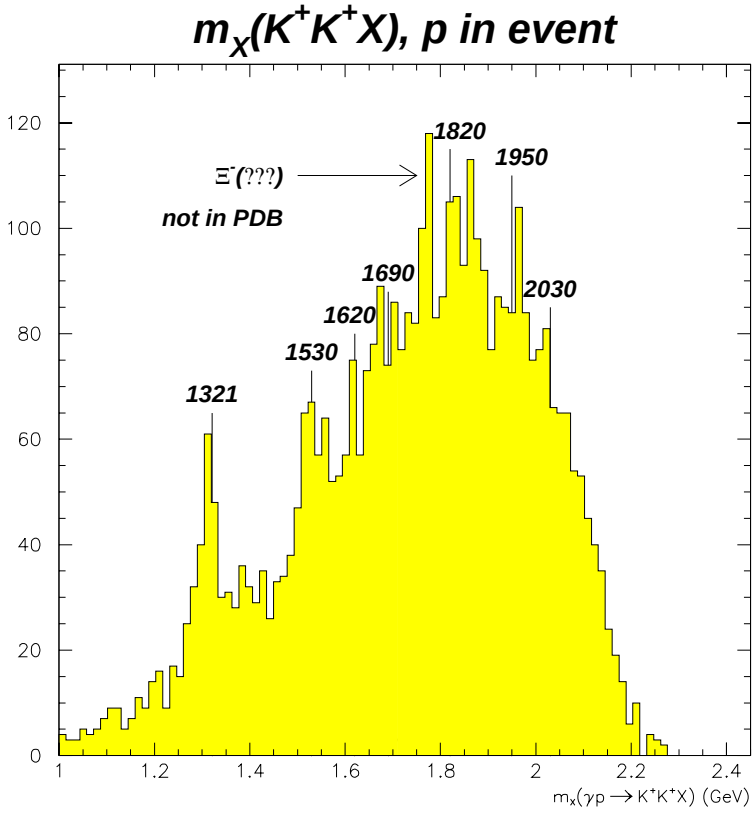

Figure 25: The missing mass plot from Fig. 24, with the additional restriction that a proton is also detected. Both the ground state $\Xi^-(1321)$ and the first excited state $\Xi^-(1530)$ are clearly seen. There are several enhancements in the plot at higher mass. Every state in the Particle Data Book up to 2030 MeV agrees well with an enhancement in the plot. There are two structures in the plot that do not appear in the Particle Data Book, at 1770 and at 1860 MeV.

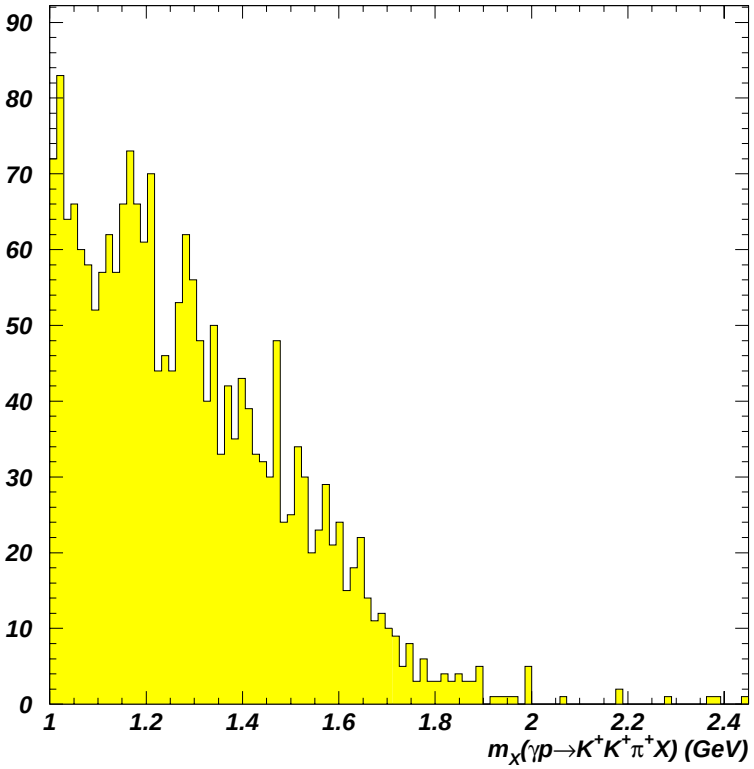

Figure 26: The missing mass in the process $\gamma p \to K^+K^+\pi^+X$ from the *g6b* data set. A peak at 1860 MeV would confirm the NA49 result.

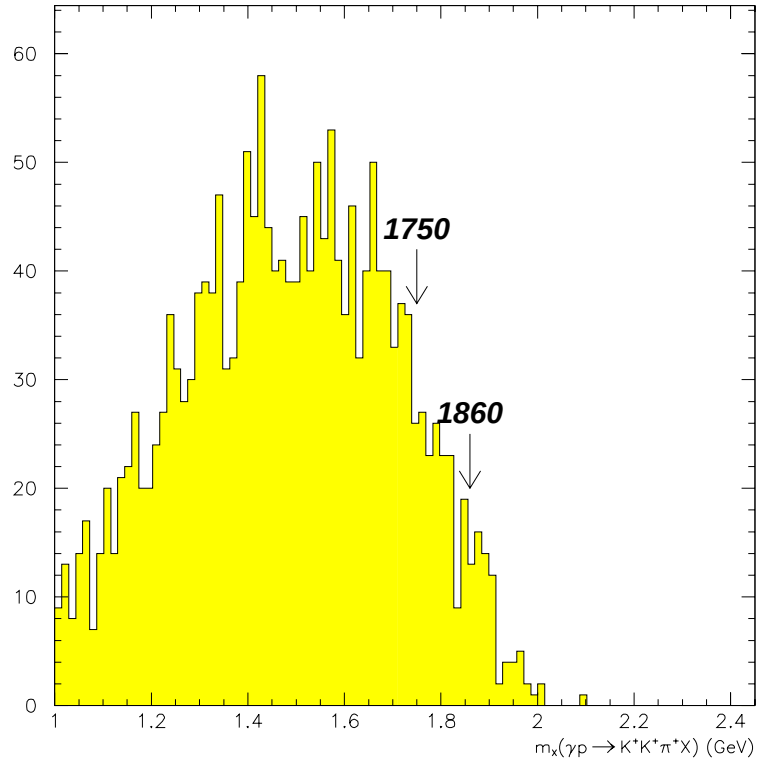

Figure 27: The missing mass in the reaction $\gamma p \to K^+K^+\pi^+X$ from the *g6c* data set. The arrows mark the original Jaffe/Wilczek prediction at 1750 MeV and the NA49 result at 1860 MeV.

3 Estimated event yield

We may estimate the expected number of events we will obtain from the Super-g run by looking at our g6c results, and by making a simple assumption about the production of the Ξ_5. From Fig. 25, we observe structure at approximately 1860 MeV. If we treat this as the $\Xi_5^-(1862)$, we may fit a polynomial background under this structure, and extract approximately 30 events in the peak. This histogram is for the process $\gamma p \to K^+K^+X; X \to pX'$. By requiring the detection of the proton from the decay chain of the Ξ^-, we reduce our sample size. We may estimate the amount of this reduction by looking at the ground state peak.

If we fit a polynomial background to the region of the ground state Ξ^- in Fig. 25 plus a gaussian peak, we extract 81 events in the peak. A similar fit to Fig. 24 gives a total of 335 events. Assuming this same ratio holds for the structure at 1860 MeV, we estimate that there are 125 $\Xi_5^-(1862)$ events in Fig. 24. With the planned running conditions of the Super-g run, we expect a factor of 12 in luminosity over the *g6c* run, from which we estimate that we will get a total of 1500 $\Xi_5^-(1862)$ events.

To estimate the number of $\Xi_5^{--}(1862)$ we will see in the Super-g run, we presume that the Ξ_5^{--} is produced by the decay of a heavier Ξ^-. Fig. 28 shows the four plots used to establish the NA49 signal. A comparison of Figs. 28a and c indicates that the production of the $\Xi_5^-(1862)$ appears to be of the same order of magnitude as that of the $\Xi^-(1530)$. From this, we will make the assumption that all excited Ξ states have the same cross section. The Ξ^- may decay to either $\pi\Xi$ or $\overline{K}\Lambda$. Based on the number of s quarks in the Ξ, we estimate that the ratio of the decay widths $\Gamma(\Xi \to \pi\Xi)/\Gamma(\Xi \to \overline{K}\Lambda) = 1/4$. Based on the Clebsch-Gordan coefficients, we then get $BR(\Xi^- \to \pi^-\Xi_5^{--}) = 0.125$. From this, we estimate that we will see a total of 200 $\Xi_5^{--}(1862)$ events in the Super-g run.

4 Conventional Ξ Physics

It is important to recognize that in addition to looking for exotic Ξ_5's, we will also use the data from the Super-g run to look for conventional three-quark Ξ states. This importance of this study is underscored by the fact that the Ξ sector of baryon spectroscopy is only poorly known. When studying exotic particles, one of the most important tests that can be made is to compare their properties with those of non-exotics. This cannot yet be done with the Ξ_5, since the properties of the non-exotic states are largely unknown. A large amount of high-quality data is needed in order to make inroads in this study.

5 Effect of a new Start Counter

In the studies of Ξ physics in CLAS to date, specifically the *g6c* data run, our progress has been limited by the properties of the start counter. This detector has three elements to cover the entire CLAS detector; the simplest event topology for Ξ photoproduction consists of $\gamma p \to K^+K^+\Xi^- \to K^+K^+\pi^-\Lambda \to K^+K^+\pi^-\pi^-p$, or five charged particles. Cleanly identifying an event such as this requires much greater granularity in the start counter. The only way we have been able to work with this is by either running at low luminosity,

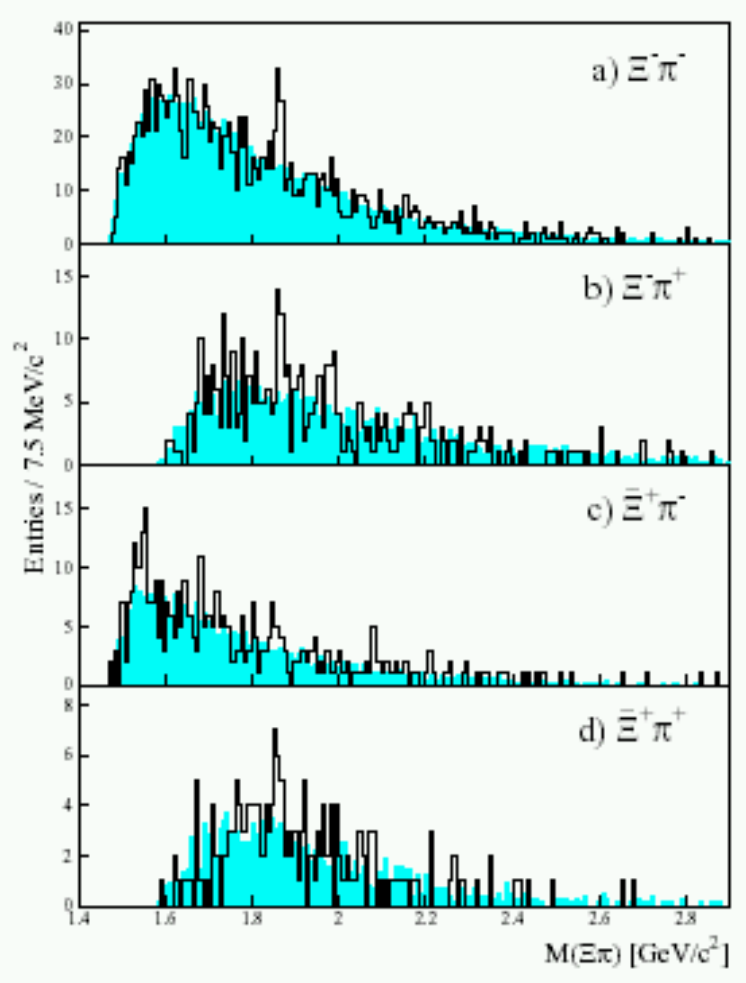

Figure 28: The results from [37], showing the various $\Xi\pi$ invariant mass plots comprising their signal.

such as in *g6a* or *g6b*, or by applying extra cuts to the event, such as the requirement to see the decay proton in *g6c*. By improving the start counter, we will be able to take data at higher rates, while still maintaining the ability to separate pions from kaons, which will improve our spectra immensely.

Part III
Experimental Conditions

1 Start Counter and Rates

The CLAS photon run g6c ran at the highest photon rates used thus far at Jefferson Laboratory. This experiment ran at a tagged photon flux of $5 \times 10^7/sec$, and at this rate each of the three elements of the Start Counter fired at a rate of about 200 kilohertz, while the total tagger OR rate was 10 Megahertz. For the physics program of g6c, only the top 12 T-counters of the tagger were used; this OR rate was approximately 1 Megahertz. An asynchronous trigger coincidence was formed between the Start Counter OR and the tagger OR, with a gate of about 15 nanoseconds. This coincidence was then put in with a coincidence of the CLAS time-of-flight counters, with a sector multiplicity of 2 and a gate of about 100 nanoseconds to form the Level 1 trigger. These triggers were subsequently processed by a crude sector tracking algorithm (Level 2) to form the data acquisition trigger. This trigger rate was approximately 1.5 kilohertz.

The accidental trigger rate of a two-component coincidence for individual rates f_1 and f_2, with a gate of Δt is approximated by:

$$Rate \sim \Delta t f_1 f_2 \tag{1}$$

g6c ran with 2 of 3 Start Counter elements in coincidence (15 nanoseconds) with the high energy end of the tagger, which gives an accidental trigger rate of order 10 hertz. However, much of the background can also be correlated hits in the Start Counter from untagged photons: this rate can be of the order of 10^5. It is this rate that is then put in coincidence with the CLAS detectors, for example time-of-flight multiplicity, with a 100 nanosecond gate.

The triggering concept here is a bit different. The Start Counter envisioned in Fig. 29 is nearly hermetic and finely segmented with approximately 100 channels, so we may trigger on Start Counter multiplicity ≥ 2, which cuts out pair production and limits the trigger to $E_\gamma > .5$ GeV, and with a tight time gate as the Start Counter is small and just a few centimeters from the target. For accidental rate estimates we extrapolate the Geant simulation of Guidal, Marchand, and Smith. From this we estimate Start Counter rates to be about 8 MHz, 90% from Compton scattering and 10% from pair production. Thus the single counter rate is 80 kHz. In addition, we have measured Start Counter rates from g6c; these rate estimates are consistent. The 3-fold accidental coincidence, with a 10 nsec coincidence gate, is estimated to be:

$$Rate \sim (10^{-8})^2 (100^3)(8 \times 10^4)^3 \sim 51200 \tag{2}$$

Thus we have a 50 kHz accidental rate *without the tagger in the trigger.* To this we add CLAS time-of-flight multiplicity = 3. The time-of-flight singles rate is about 5 kHz under these conditions- we suspect most of this rate comes from spray from the tagger, and may be reduced by shielding upstream. A three fold coincidence with a 100 nsec gate:

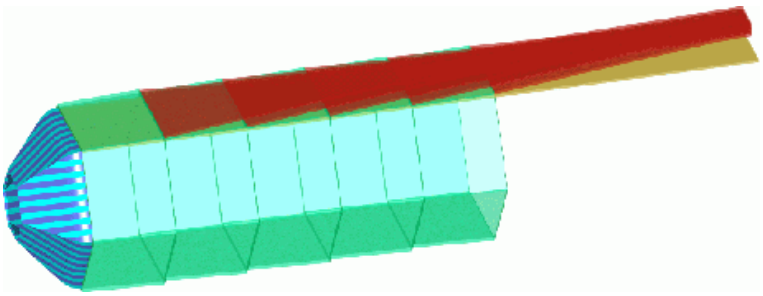

Figure 29: Proposed Start Counter

$$Rate \sim (10^{-7})^2 \times (5 \times 10^3)^3 \times 288^3 \sim 30kHz \tag{3}$$

Adding these two in coincidence gives a Level 2 accidental trigger rate of about 150 Hz which is negligible . If the CLAS time-of-flight multiplicity is relaxed to 2, the accidental rate increases to about a kilohertz.

The 3-prong rate ($\sim 90\mu barns$) is estimated to be of the order of 12 kilohertz, but includes *desirable physics events*. This rate will be put in coincidence with the CLAS time-of-flight multiplicity, which includes geometric efficiency, and is of the order of 10%, for a total real trigger rate of order 1-2 kilohertz. When added to the above accidental rate, the total is well within the current limits of the CLAS data acquistion system, which is about 4 kilohertz, and is expected to increase by 100% in the next year. The event rate to tape may be decreased further by implementing the CLAS Level 2 tracking algorithm, which identifies charged tracks in the drift chambers. Futher reductions in total trigger rate may be obtained by correlating hits in the segmented Start Counter to time-of-flight elements, which is not possible in the current CLAS photon configuration.

2 Running Conditions

The high-luminosity experimental run being proposed here encompasses a broad range of physics topics over a wide energy range. As such, the running conditions for this anticipated running period have not yet been completely defined, although some considerations are apparent.

In order to achieve higher statistics over previous experimental runs it is intended to run at a higher luminosity. While the tagger has already been run successfully at its maximum rate (in g6c), it is not possible to run with a higher tagged photon flux ($5 \times 10^7/sec$). Even at this rate about 10% of the triggers have 2 tagged photons with the same accelerator RF bucket. Thus, to increase luminosity a 40 cm liquid hydrogen target will be used.

CLAS has already successfully taken data over a target range of over one meter with excellent track reconstruction. The current Start Counter surrounding the target is not long enough to accomodate the longer target length, so we plan to build a longer counter

with more sectors, which will greatly improve beam photon identification. This will allow the very high beam fluxes anticipated while preventing high rate backgrounds from contaminating the rarer channels of interest which we will be investigating (see Section V. B).

The target will be located upstream of the nomial CLAS center in order to improve acceptance of the low momentum processes which dominate the Θ^+ and Ξ production, but not upstream enough to lose small t recoil protons which bend out of the CLAS active region. Because we are looking for narrow states, mass resolution is an important consideration. To reduce signal to noise, we anticipate running CLAS at 3/4 of its maximum field. Monte carlo acceptance studies, however, are currently being pursued to determine the optimum combination of target position and spectrometer magnet field setting.

The photon beam itself will be configured as for the g6c run, that is an electron beam energy on 40 nanoamps at the highest energy available above 5.7 GeV. The beam will be incident on a 3×10^4 radiator. This will correspond to a luminosity of nearly 10^{33} cm^{-2} - sec^{-1}. The raw sensitivity over 40 days of running will be 300 events/pbarn.

Part IV
Conclusions

In this document we have proposed a comprehensive study of pentaquarks on a proton target. The successes we have had analyzing g6 run data give us the confidence to propose an experiment which will utilize photons ranging in energy from below threshold to the highest available at JLab with a 5.75 GeV electron beam, and with a new segmented start counter to achieve luminosities an order of of magnitude higher than any previously available. The combination of both these experimental conditions, will allow us to break new ground simultaneously on several crucial issues in the study of pentaquarks. The questions which we will study are the following:

I. Properties of the Θ^+.

Production mechanism. In our analysis of the g6 data two reaction mechanisms suggested themselves. One is the pion exchange t-channel with the possible formation of a resonance which decays into a Θ^+ and a kaon. The other is via a K^* t-channel, with the direct production of the Θ^+. The two production mechanisms of these can only be studied with a high rate, maximum energy photon beam.

Decay channels: spin and parity. Our simulations show that, having extracted the production mechanism, the decay angular distributions will contain a very strong signature of the spin; that is we will be able to determine whether the Θ^+ has a spin of 1/2 or 3/2. The signature for the parity is somewhat more ambiguous. However, within the framework of various model calculations the cross sections and decays differ by an order of magnitude between the Θ^+ having positive and negative parity.

Our MC simulations, together with our experiences with the g1c running period, show that the integrated luminosities obtainable will yield more than an order of magnitude more data than ever previously available. As shown in the text, this will allow us to obtain absolute cross sections, as well as t and θ distributions which will allow us to make definite statements about the reaction mechanism and spin, and perhaps about parity as well.

II. Production of the Ξ_5.

One of the most important problems in the study of pentaquarks is the verification of the existence of the four members of the Ξ_5 multiplet. The highest beam energy available, in this case 5.75 GeV, is essential to observe them since their threshold for production ranges from 3.9 to 4.7 GeV. The g6 data shows much structure in the region of the NA49 observation of the Ξ_5. However, the large pion background makes it difficult to make any definite statements. Both high luminosity combined with excellent pion background rejection is necessary. This will be made possible by the construction of the new highly segmented start counter in CLAS. We estimate that with the proposed integrated luminosities, we expect to observe a significant number of Ξ_5, possibly as high as 200 and 1500 for the Ξ_5^{--} and Ξ_5^- respectively. These numbers would allow us to obtain distributions, as in the case of the Θ^+, which would give us information about their production and decay mechanisms.

In conclusion, the proposed experiment, with its unique experimental conditions of high energy and high luminosity will allow us to discover and characterize pentaquark states as never before possible. Finally we wish to emphasize that this experiment will share running time with another current proposal to study the photoproduction of exotic mesons ("Search for New Forms of Hadronic Matter in Photoproduction", P. Eugenio, C. Salgado, D. Weygand). In the same experiment we have an opportunity to investigate both exotic baryons and exotic mesons.

References

[1] T.Nakano et al., Phys. Rev. Lett. 91, 012002 (2003); T. Nakano et al. (LEPS Collaboration) e-Print Archive: hep-ex/0301020

[2] V. Barmin et al, Phys.At.Nucl.,66:1715-1718 (2003); e-Print Archive: hep-ex/0304040.

[3] S. Stepanyan et al., e-Print Archive: hep-ex/0307018, to be submitted to PRL.

[4] V. Kubarovsky and S. Stepanyan, presented at the Conference on the Intersections of Particle and Nuclear Physics (CIPANP2003), New York, NY, USA, May 19-24, 2003, e-Print Archive: hep-ex/0307088

[5] V. Kubarovsky et al., to be submitted to PRL.

[6] J. Barth et al., e-Print Archive: hep-ex/0307083.

[7] A.E.Asratyan et al., e-Print Archive: hep-ex/0309042.

[8] NA49 collaboration, C. Alt et al., e-Print Archive: hep-ex/0310014.

[9] D. Diakonov, V. Petrov, and M. Polyakov, *Z. Phys.* A **359**, 305 (1997)

[10] D. Diakonov and V. Petrov, e-Print Archive: hep-ph/0310212.

[11] H. Walliser, Nucl. Phys. A **548**, 649 (1992).

[12] H. J. Lipkin, Nucl. Phys. A **625**, 207 (1997)

[13] H. Walliser and V. B. Kopeliovich, arXiv:hep-ph/0304058.

[14] F. Stancu and D. O. Riska, arXiv:hep-ph/0307010.

[15] S. Capstick, P. R. Page and W. Roberts, decaying partners," arXiv:hep-ph/0307019.

[16] N. G. Kelkar, M. Nowakowski and K. P. Khemchandani, J. Phys. G **29**, 1001 (2003)

[17] B. G. Wybourne, arXiv:hep-ph/0307170.

[18] A. Hosaka, arXiv:hep-ph/0307232.

[19] R. L. Jaffe and F. Wilczek, arXiv:hep-ph/0307341.

[20] M. Karliner and H. J. Lipkin, arXiv:hep-ph/0307243.

[21] S. L. Zhu, arXiv:hep-ph/0307345.

[22] S. Nussinov, arXiv:hep-ph/0307357.

[23] D. Borisyuk, M. Faber and A. Kobushkin, arXiv:hep-ph/0307370.

[24] L. Y. Glozman, arXiv:hep-ph/0308232.

[25] S. Capstick, P.R. Page, W. Roberts, e-Print Archive: hep-ph/0307019.

[26] P.R. Page, e-Print Archive: hep-ph/0310200.

[27] R. Jaffe and F. Wilczek, e-Print Archive: hep-ph/0307341.

[28] W. Liu and C.M. Ko, e-Print Archive: nucl-th/0‘308034.

[29] W. Liu and C.M. Ko, e-Print Archive: nucl-th/0309023.

[30] S.I. Nam al., e-Print Archive: hep-ph/0308313.

[31] Y. Oh et al., e-Print Archive: hep-ph/0310019.

[32] W. Liu, C.M. Ko,V. Kubarovsky, e-Print Archive: nucl-th/0310087.

[33] M. Polyakov, private communication, 2003.

[34] M. Polyakov, private communication, 2003.

[35] M. Guidal, M, Vanderhaeghen, and M. Polyakov.

[36] P. Page, arXiv:hep-ph/0310200.

[37] C. Alt *et al.*, arXiv:hep-ex/0310014.

[38] W. Liu, presentation at Penta-quark 2003 workshop.